Food Innovation and Advances

ARTICLE

Open Access

https://doi.org/10.48130/fia-0025-0001

Food Innovation and Advances **2025**, 4(1): 19–30

Resveratrol promotes spherical nano-self-assembly of egg white protein to enhance emulsification performance

Yuxin Kang[1#], Nan Xiao[1#], Haodong Wu[1], Zhixiong Pan[1], Weiwei Chen[2] and Minmin Ai[1,3*]

[1] *The National Center for Precision Machining and Safety of Livestock and Poultry Products Joint Engineering Research Center, College of Food Science, South China Agricultural University, Guangzhou 510642, China*

[2] *College of Food and Bioengineering, Henan University of Science and Technology, Luoyang 471000, China*

[3] *Guangdong Provincial Key Laboratory of Food Quality and Safety, College of Food Science, South China Agricultural University, Guangzhou 510642, China*

[#] Authors contributed equally: Yuxin Kang, Nan Xiao

* Corresponding author, E-mail: scauaiminmin@scau.edu.cn

Abstract

In this paper, using a single-step method, resveratrol (RES)-loaded egg white protein (EWP) nanospheric particles were successfully prepared. The micelle behavior, micromorphology, molecular structure changes, and emulsifying properties of the nanoparticle were analyzed, and the molecular interaction between EWP and RES and the environmental response stability of the nanoparticle was characterized. The results show that I_{373}/I_{385} dropped from 1.1 to about 0.8, indicating that high concentration of ethanol induced EWP to form a more hydrophobic and less polar structure. RES promoted the uniformity of the nanoparticle and formed a tightly-packed spherical three-dimensional structure by characterizing microstructure. Raman and infrared spectroscopy revealed enhanced hydrogen bonding between EWP and RES, increased g-g-g and t-g-t disulfide bonds, and the formation of three-dimensional helical structures due to the opening of flexible structural intervals. Molecular docking analysis identified hydrogen bonds and hydrophobic interactions as the main forces facilitating the binding between RES and EWP. Particle size analysis showed that $D_{3,2}$ decreased from 30.51 to 17.88 μm, indicating better emulsion stability. The preservation of RES at 0.4 mg/mL was 94.49% in 50 mM NaCl and 83.68% in 500 mM NaCl, with no significant stability change ($p > 0.05$) over 48 h, revealing a concentration dependence of salt ions and storage stability of RES in the nanoparticle. This study establishes a foundation for exploring the incorporation of high-value hydrophobic compounds into EWP.

Citation: Kang Y, Xiao N, Wu H, Pan Z, Chen W, et al. 2025. Resveratrol promotes spherical nano-self-assembly of egg white protein to enhance emulsification performance. *Food Innovation and Advances* 4(1): 19–30 https://doi.org/10.48130/fia-0025-0001

Introduction

Resveratrol (3,5,4′-trihydroxystilbene, RES) is a polyphenolic compound present in various plants, including berries, grapes, peanuts, and wine[1]. RES reduces inflammation, inhibits tumor growth, and protects the heart and blood vessels. However, RES exhibits poor chemical stability depending on environmental factors such as temperature and pH. That is, RES is stable under acidic conditions and degrades rapidly under neutral or alkaline environments[2]. The half-life of trans-RES was found to be 329 d at a pH of 1.2 but only 3.3 min at a pH of 10.0[2]. The degradation degree of trans-RES was found to be 17% at 125 °C but increased to 70% at 175 °C[3]. Environmental stresses limit the use of RES in the food and medical industries due to its instability. Hence, the preparation of controlled, green, and safe nanoparticles to reduce the environmental sensitivity of RES is an important focus at present. Such systems are essential for the practical utilization and controlled development of RES.

Current food-grade encapsulation materials are mainly composed of proteins, polysaccharides, and lipids, and exhibit excellent biodegradability and high human safety and nutritional value. Such materials have been widely adopted to carry, encapsulate, protect, and deliver various bioactive compounds with improved stability and utilization. For instance, Chen et al.[4] used maize protein, pectin, and chitosan to synthesize particles with a multilayer structure to transport and encapsulate coenzyme Q10 and piperine. Peñalva et al.[5] enhanced the oral availability of RES by encapsulating it with casein, achieving significantly higher availability compared to an oral solution of RES. Although these nanoparticles were found to have good encapsulation and stabilization effects during laboratory testing, several limitations were observed, including gelation of casein, susceptibility to pH, and high equipment and solvent requirements for the preparation of corn protein-nanoparticles. Thus, these systems are not widely used industrially. In contrast, EWP has attracted the attention of scientists due to its biocompatibility, low cost, and ability to be applied without additional processing, and thus, is frequently employed in biomaterial delivery[6,7]. Kleemann et al.[8] applied EWP to prepare aerogels to encapsulate fish oil. The findings indicated a greater loading capacity compared to whey protein and casein. Zhu et al.[9] prepared various nanostructural EWPs to embed vitamins A, D, and E, demonstrating the excellent anti-degradation stability of the prepared systems. Despite the excellent performance of EWP nanoparticles, EWP still has limitations[10]. Ovalbumin, the primary protein in egg whites, comprises approximately 50% hydrophobic amino acids. However, a significant majority of these hydrophobic residues are situated deep within the molecular framework, leaving only a minor fraction exposed on the surface. Consequently, this arrangement leads to lower amphiphilicity and diminished emulsification capacity of EWP. The delivery of hydrophobic active compounds is challenging, necessitating the careful selection of appropriate encapsulation materials to ensure their stability. In response to the above problems, we were surprised to find that the depolymerization-aggregation process of EWP during ethanol induction led to EWP nanospheres with better stability.

Preliminary research by our research team revealed that EWP can be applied as a carrier for pro/hydrophobic active compound

nanoparticles[11]. Through pre-experiments, we found that EWP exhibited excellent RES encapsulation properties. Therefore, we investigated the effects of RES on the molecular structure and functional activity of EWP-promoted spherical nanoparticles induced by ethanol. This study provides a research and theoretical basis for improving RES utilization and expanding EWP-derived nanoparticles.

Materials and methods

Material

Newly laid eggs, each within the weight range of 55 to 65 g, were sourced from a grocery store in Guangzhou, China. RES (of 98% purity) was acquired from Xi'an Qiuhe Biotechnology Co., Ltd. (Xi'an, China). 8-aniline-1-naphthalenesulfonic acid (ANS) and 5,5′-dithiobis-(2-nitrobenzoic acid) (DTNB) were obtained from Sigma-Aldrich (St. Louis, MO, USA). All other chemical substances employed were of a standard suitable for analytical purposes.

Preparation of EWP nanoparticles loaded with RES

Eggs were thoroughly washed and the EWP were extracted. The EWP was homogenized at 1,500 rpm for 10 min and then refrigerated for 4 h. After removing the surface foam, the nitrogen content, representing protein concentration, was determined using the Kjeldahl method. The concentration of EWP was standardized to 10% (w/w), and a trace amount of sodium azide, specifically 0.02% by weight, was incorporated to prevent bacterial contamination. RES was dissolved in an ethanol solution with a volume fraction of 30% to 80% (v/v) to prepare concentrations ranging from 0.01 to 0.40 mg/mL. The EWP was also adjusted to different concentrations, spanning from 0.1 to 2.0 mg/mL. The RES ethanol solution was thoroughly combined with the EWP solution in equal volumes and then allowed to rest and stabilize before being refrigerated. A subset of these samples underwent ethanol removal via rotary evaporation at a temperature of 55 °C, followed by a 72-h freeze-drying process.

Interaction of EWP with resveratrol

Pyrene fluorescence

The fluorescence of pyrene was quantified by preparing a pyrene-acetone mixture with a pyrene concentration of 200 μM. To this mixture, 2 mg/mL of EWP solution was introduced at varying ethanol concentrations. Subsequently, a suitable volume of the pyrene-acetone mixture was added to achieve a final pyrene concentration of 1 μM in the samples. After agitating the samples for 12 h to ensure thorough mixing, the fluorescence spectra were recorded. For the fluorescence measurements, an excitation wavelength of 335 nm was used, and the emission was monitored over a range of 350 to 600 nm.

Molecular force

The changes in molecular force in the nanoparticle were characterized by sulfhydryl content, molecular flexibility, and surface hydrophobicity. Other experimental details are listed in the Supplementary File 1.

Intrinsic fluorescence

EWP was prepared at 2 mg/mL, and RES concentrations varied from 0 to 0.4 mg/mL. The experimental setup utilized an excitation wavelength of 280 nm and an emission spectrum ranging from 290 to 500 nm. The intrinsic fluorescence of RES was evaluated by maintaining a constant RES concentration of 0.1 mg/mL while varying the EWP concentration from 0 to 2 mg/mL. Fluorescence measurements were performed using a 320 nm excitation wavelength and an emission spectrum between 330 and 550 nm. The slit widths for both excitation and emission were maintained at 5 nm[12].

Molecular docking

The 3D structure of ovalbumin (PDB ID: 1OVA) was obtained from the RCSB Protein Data Bank. Concurrently, the 3D structure of RES was obtained from the PubChem database. Molecular docking analyses were conducted using Autodock Vina software, version 1.1.2[13]. The grid for the docking simulations was configured as a cubic lattice with dimensions of 3.8 nm on each side. The protein's search space was defined with coordinates centered at 22.7 Å × 61.6 Å × 18.9 Å, and docking was performed with an exhaustiveness of 1000. The Lamarckian Genetic Algorithm was employed for the docking calculations. Subsequently, the most favorable docking configurations were selected and further analyzed using the open-source PyMOL software, version 2.5.

Turbidity

Twenty milligrams of freeze-dried nanoparticles were added to 10 mL of deionized water. The solution's turbidity was evaluated by measuring its absorbance at 600 nm with a Shimadzu UV2600 spectrophotometer. Each experimental trial was performed three times to ensure reproducibility.

Encapsulation efficiency

Fresh specimens were centrifuged at 5,000 rpm for 30 min at 4 °C. This process was carried out to separate and collect a supernatant that contained unbound RES. The concentration of the free RES in the supernatant was ascertained by referencing a standard curve, which was calibrated using absorbance measurements at a wavelength of 360 nm. This curve was generated by assessing the absorbance of RES across a spectrum of concentrations, from 1 to 25 μg/mL. The encapsulation efficiency of RES was then determined using the following formula:

$$Encapsulation\ efficiency\ (\%) = \frac{Total\ resveratrol - Free\ resveratrol}{Total\ resveratrol} \times 100\% \quad (1)$$

Raman

The freeze-dried samples were mounted onto glass slides and then covered with aluminum foil to protect them from light. Raman spectroscopy measurements employed a 785 nm excitation wavelength and a 300 mW emission power. Raman spectra were obtained across a wavenumber range of 400 to 1,800 cm^{-1}. Scanning was repeated at least three times for each sample. Baseline correction and attribution of the Raman spectrum were performed by OMINIC software.

The normalization procedure employed the Raman peak at 1,004 cm^{-1}, which corresponds to the internal standard of phenylalanine, to account for the intensity fluctuations observed in each Raman peak. The spectral fitting was carried out using two software packages: Origin 9.1 and PeakFit 4.12. The numbers of buried tyrosine (N_{buried}) and exposed tyrosine ($N_{exposed}$) were calculated as follows:

$$0.5N_{buried} + 1.25N_{exposed} = I_{850}/I_{830} \quad (2)$$

$$N_{buried} + N_{exposed} = 1 \quad (3)$$

Interaction mechanism and morphology

To better verify the physicochemical properties of nanoparticles, a series of experiments at different resveratrol concentrations were performed. X-ray diffraction (XRD) and Fourier-transform infrared (FTIR) spectroscopy were employed to elucidate the interaction mechanisms within the nanoparticles. Transmission electron microscopy (TEM) and atomic force microscopy (AFM) were utilized to analyze the shape and structure of the nanoparticles. Other experimental details are listed in the Supplementary File 1.

Interfacial tension and emulsifying capacity of nanoparticles

The nanoparticles were reconstituted in deionized water to a concentration of 1 mg/mL. The interfacial tension of the nanoparticles was measured at 25 °C using the platinum ring method with a DSA100 instrument from Krüss GmbH (Hamburg, Germany). The nanoparticles were dissolved overnight to achieve a 0.5% (w/w) concentration. An emulsion was prepared by homogenizing 40 mL of nanoparticle suspension with 10 mL of corn oil at 10,000 rpm for 2 min. Following homogenization, 100 μL of the emulsion was extracted from the bottom layer and combined with 4.9 mL of a 0.1% sodium dodecyl sulfate (SDS) solution. The absorbance of the mixture was recorded at 500 nm both initially and after 10 min. The emulsifying activity index (EAI) and stability index (ESI) of the emulsion were calculated using the formulas in Eqns (4) and (5), respectively.

$$EAI\ (M^2/g) = \frac{2 \times 2.303 \times DF \times A_0}{C \times 0.2 \times 10000} \quad (4)$$

$$ESI\ (min) = \frac{A_0}{A_0 - A_{10}} \times 10 \quad (5)$$

where, DF is set at 100. The initial concentration of the hydrolysates is denoted by C (g/mL). The emulsion is formed using 20% corn oil. The absorbance readings, A_0 and A_{10}, indicate the optical density of the diluted emulsion at the initial time and after 10 min, respectively.

Characterization of emulsion properties

The emulsions were subjected to laser diffraction analysis to determine the average particle size. This measurement was conducted at 25 °C and a stirring speed of 1,200 rpm. The refractive indices were set at 1.33 for water as the dispersing medium and 1.462 for the particles. The average surface particle size ($D_{3,2}$), as determined, was indicative of the overall particle size distribution. The emulsion was diluted by a factor of 200 before measuring the ζ-potential using a nanoparticle size potentiostat. The samples were allowed to equilibrate for 120 s before testing, with the temperature maintained at 25 °C. Freshly prepared emulsions were centrifuged at 12,000 g for 1 h at 20 °C. The lower aqueous phase was extracted with a pipette through a 0.45 μm membrane filter. The protein content in this phase was quantified using the Coomassie Brilliant Blue method, with a calibration curve based on bovine serum proteins. Similarly, the resveratrol content was determined following a previously established method, and the interfacial resveratrol content was calculated accordingly.

Stability of RES in the spherical nanoparticles

Spherical nanoparticles with varying RES concentrations (0.01–0.40 mg/mL) were evaluated for ionic stability at NaCl concentrations ranging from 0-500 mM and for storage stability at 40 °C over 48 h. RES content was assessed using a previously established method, and the RES residual rate was calculated.

Data analysis

Each experimental trial was repeated three times to ensure consistency and reliability. Statistical evaluation was conducted using analysis of variance (ANOVA) and Duncan's multiple range test for mean comparisons. The analyses were performed using IBM SPSS software, version 21.0. $p < 0.05$ was set to reflect statistical significance. The graphical representations of the findings were created using Origin software, version 9.1.

Results and discussion

Micellar behavior of ethanol-induced EWP

Pyrene is a strongly hydrophobic fluorescent probe and the ratio of the third to fifth peak (I_{373}/I_{385}) decreased with reductions in the microenvironment polarity and increases in the hydrophobicity where pyrene was located[14,15]. Figure 1a illustrates the changes in pyrene fluorescence intensity within EWP as the ethanol concentration is altered. The fluorescence intensity of pyrene decreased as ethanol concentration increased. The significant decrease in pyrene fluorescence intensity at ethanol concentrations below 50% (v/v) indicates that ethanol modifies the protein surface group distribution, leading to fluorescence quenching of pyrene. Fluorescence intensity reductions were negligible at ethanol concentrations exceeding 50%, likely due to protein denaturation caused by high ethanol levels, disrupting the EWP-pyrene complex. The I_{373}/I_{385} of pyrene in sodium phosphate buffer was 1.1. No statistically significant variations were observed ($p > 0.05$) when the ethanol concentration ranged from 10% to 30%. At these concentrations, ethanol molecules predominantly existed in monomeric form within the aqueous solution, and their increased presence had a minimal impact on the microenvironment surrounding the dispersed pyrene molecules. However, a significant decrease in the I_{373}/I_{385} ratio was noted ($p < 0.05$) as the ethanol concentration increased to 40%–50%. This change suggests that EWP started to aggregate, causing pyrene molecules to migrate towards the hydrophobic regions within the nanoparticles. Consequently, the microenvironment experienced a reduction in polarity and an increase in hydrophobicity. As the ethanol concentration increased to 70%, I_{373}/I_{385} rapidly decreased to about 0.8, indicating that a more hydrophobic and less polar microenvironmental structure was formed at this point. Combined with the change of pyrene fluorescence intensity and I_{373}/I_{385}, the most appropriate ethanol induction concentration is 50%.

Encapsulation efficiency of EWP-loaded RES

The appearance of EWP loaded with RES is shown in Fig. 1b. As the RES concentration increased, the nanoparticle changed from turbid to more transparent. Protein aggregation often results in increased turbidity, which can qualitatively assess the extent of aggregation. The nanoparticle turbidity is shown in Fig. 1d. Turbidity significantly decreased ($p < 0.05$) in groups with 0.3 and 0.4 mg/mL RES, whereas no significant change was observed in groups with 0.02 and 0.05 mg/mL RES. This suggests that adding RES resulted in the uniform dispersion of EWP and the formation of a stable and homogeneous nanoparticle.

The encapsulation efficiency is an important indicator for evaluating a carrier's ability to encapsulate functional compounds. Figure 1c depicts the influence of varying protein and ethanol concentrations on the encapsulation efficiency of RES at a fixed concentration of 0.2 mg/mL. When the ethanol concentration was 30%, the encapsulation rate of RES increased from 25.82% to 60.56% as the EWP concentration increased. This indicates that the carrier proportion facilitated RES embedding through hydrogen bond formation between EWP and RES. At 0.4 mg/mL RES, the encapsulation efficiency initially rose and then declined with ethanol concentrations increasing from 30% to 80%. The maximum encapsulation rate of RES occurred at 0.4 mg/mL EWP and 50% ethanol, reaching 84.14%. This suggests that an appropriate increase in ethanol leads EWP to expose more -OH which can interact with RES through intermolecular hydrogen bonds[16], while high ethanol concentrations denature the protein, thus reducing the RES encapsulation rate. Meanwhile, the water solubility of RES improved with increasing ethanol concentration[16]. High ethanol concentrations disrupted hydrogen bonds, leading to further disturbance of the protein's hydrophobic regions[17]. This hindered the interaction between EWP and RES and reduced the encapsulation rate of RES.

RES modulates the molecular structure of EWP

The presence of free sulfhydryl groups is indicative of the structural alterations and functional attributes of proteins, which are

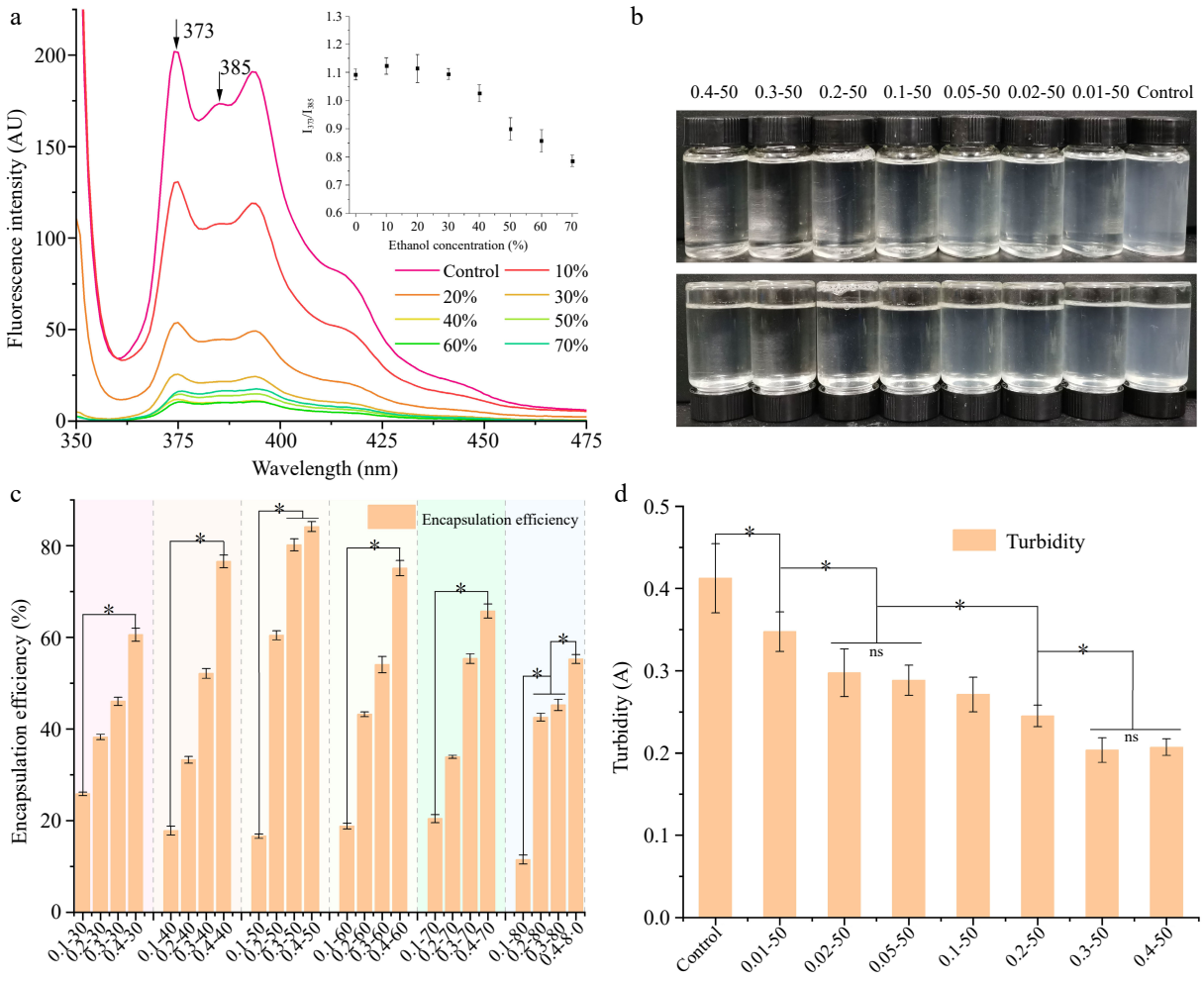

Fig. 1 (a) Pyrene fluorescence, and the interpolation shows the ratio of I_{373}/I_{385} of EWP with adding different proportion of ethanol. The (b) appearance features, (c) encapsulation efficiency, and (d) turbidity of ethanol-induced EWP with adding different proportion of RES. 0.01−50, the preceding digits are RES concentrations (mg/mL), and the following numbers are ethanol concentrations (v/v), other groups are similar. * Indicates significant difference ($p < 0.05$).

closely linked to the solubility and gel-forming abilities of proteins[18,19]. Figure 2a demonstrates a significant decrease ($p < 0.05$) in free sulfhydryl groups in EWP at RES concentrations below 0.02 mg/mL. This decrease implies that at low RES concentrations, some of the free sulfhydryl groups located on the EWP surface become encapsulated within the protein's interior. Conversely, as the RES concentration increased further, there was a notable rise in the free sulfhydryl content ($p < 0.05$). This increase suggests that the introduction of higher RES concentrations led to the exposure of EWP's molecular structure and facilitated the conversion between sulfhydryl and disulfide groups, thereby elevating the content of free sulfhydryl groups.

The adaptability of a protein's structure is intricately connected to its conformation, with a particular emphasis on the proportion of high β-turns present[20]. Figure 2b demonstrates the impact of RES addition on the molecular flexibility of EWP. The flexibility of protein molecules significantly increased ($p < 0.05$) with a higher RES proportion. This indicates that the addition of RES caused the flexible regions of EWP to expand, with more rigid structures being opened and rearranged to form flexible parts.

Surface hydrophobicity influences protein's solubility, emulsification ability, and gelling characteristics. Changes in hydrophobicity primarily result from the exposure of hydrophobic aliphatic and aromatic amino acid residues during protein unfolding[21]. Figure 2c illustrates the changes in surface hydrophobicity of EWP with the addition of RES. Surface hydrophobicity significantly decreased ($p < 0.05$) with increasing RES concentration. This observation is consistent with prior research indicating that elevated ethanol levels reduce protein surface hydrophobicity[11]. The active site of solubilized RES binds to the surface hydrophobic groups of EWP, while changes in the microenvironment encapsulate certain aromatic and aliphatic amino acids within EWP, reducing surface hydrophobicity.

Interaction between EWP and RES

The intrinsic fluorescence technique was employed to ascertain the interactions between EWP and RES, with the findings depicted in Fig. 3. Figure 3a specifically illustrates the impact of RES addition on the fluorescence spectrum of EWP. RES interacted with EWP to form complexes, reducing the intrinsic fluorescence. When the RES concentration ranged from 0–0.2 mg/mL, the fluorescence emission peak of EWP was red-shifted from 332 to 363 nm, and significant quenching occurred. This suggests that the addition of RES shifted the protein fluorescent chromophore to a more hydrophilic environment[22]. The fluorescence intensity of EWP increased significantly as the EWP concentration increased (Fig. 3b), indicating that EWP interacted with RES markedly. Further, the fluorescence emission peak was slightly blue-shifted, indicating that the number of polar groups exposed of the EWP was decreased[22].

Fluorescence quenching can result from mechanisms such as excited state reactions, molecular rearrangements, energy transfer,

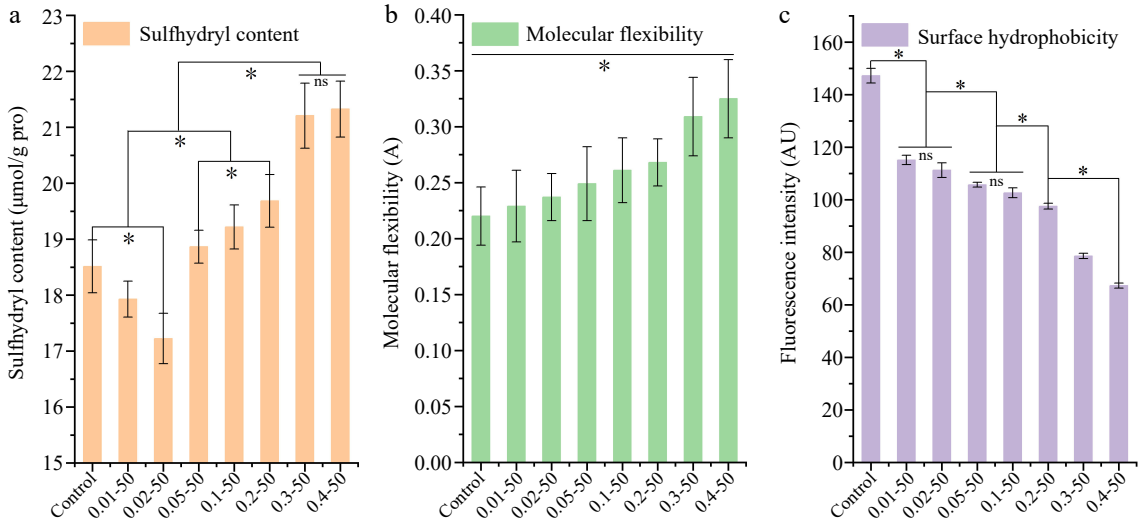

Fig. 2 The (a) sulfhydryl content, (b) molecular flexibility, and (c) surface hydrophobicity of ethanol-induced EWP with adding different proportion of RES. 0.01-50, the preceding digits are RES concentrations (mg/mL), and the following numbers are ethanol concentrations (v/v), other groups are similar. * Indicates significant difference ($p < 0.05$).

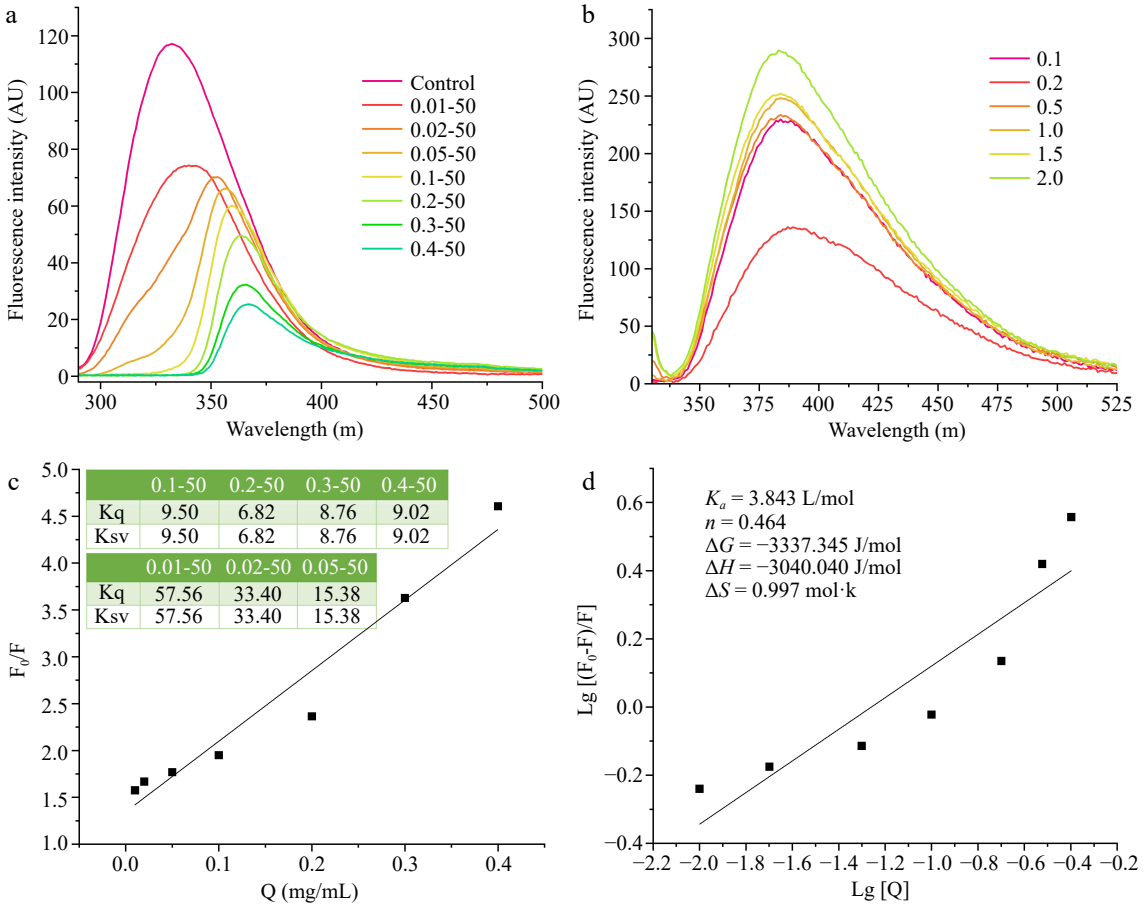

	0.1-50	0.2-50	0.3-50	0.4-50
Kq	9.50	6.82	8.76	9.02
Ksv	9.50	6.82	8.76	9.02

	0.01-50	0.02-50	0.05-50
Kq	57.56	33.40	15.38
Ksv	57.56	33.40	15.38

Fig. 3 The intrinsic fluorescence of EWP with adding different ratios of (a) RES, and different ratios of (b) EWP. (c) The Stern-Volmer curved line of the interaction of ethanol-induced EWP with adding different proportions of RES, and (d) the double logarithmic regression curve. 0.01–50, the preceding digits are RES concentrations (mg/mL), and the following numbers are ethanol concentrations (v/v), other groups are similar. 0.1–2.0 (b) is the concentration of EWP (mg/mL).

ground state complex formation, and dynamic collisional interactions. Stern-Volmer plots illustrate the relationship between fluorescence intensity with and without a quencher by plotting the ratio of initial fluorescence intensity (F_0) to quenched fluorescence intensity (F) against the concentration of RES [Q]. *Ksv* denotes the dynamic quenching constant, and *Kq* represents the bimolecular quenching constant. Figure 3c demonstrates a linear relationship for RES concentrations ranging from 0.05 to 0.3 mg/mL. The quenching rate constant of 6.82×10^9 $M^{-1} \cdot s^{-1}$ is notably lower than the maximum dynamic diffusion quenching constant of 2.0×10^{10} $M^{-1} \cdot s^{-1}$ for

biomolecule interactions. This discrepancy suggests that the fluorescence quenching of EWP by RES is primarily due to dynamic quenching[23]. The quenching behavior likely arises from conformational changes in EWP induced by the addition of RES.

The interaction between EWP and RES was analyzed using a double logarithmic plot to determine the binding affinity (*Ka*) and the number of binding sites (*n*). Figure 3d demonstrates that there was a linear relationship between Log[Q] and the concentration range from −2.0 to −0.5. The interaction type can be deduced from entropy (ΔS) and enthalpy (ΔH) changes: negative ΔS and ΔH indicate hydrogen bonding, positive ΔS and ΔH suggest hydrophobic interactions, and positive ΔS with negative ΔH imply electrostatic interactions[24]. The *Ka* of EWP and RES was 3.843 L/mol and *n* was 0.464. Further, ΔG < 0, suggesting that the bonds between EWP and RES were spontaneous reactions[25]. Moreover, ΔS was 0.997 mol·k, ΔH was −3,040.040 J/mol, ΔS > 0, and ΔH < 0, indicating that the interaction between EWP and RES was an electrostatic interaction.

Crystallization behavior and microstructure of nanoparticles

The crystallinity degree was detected by XRD. The XRD spectrum is shown in Fig. 4a. The major peak in the spectrum at 19.7° reflects the ovalbumin peak[26]. As the RES concentration increased, new peaks appeared in the spectrum, such as 8.5°, 22.3°, 23.1°, 26.0°, and 31.0°, while some peaks disappeared, such as 43.5°, 44.3°, 50.5°, and 74.5°. This indicates that the addition of RES significantly affected the crystallinity of EWP. The XRD-fitted peaks from 15.0° to 60.0° are shown in Fig. 4b. As RES increased, the peaks at 22.3°, 23.1°, and 31.0° became sharper and narrower, likely due to the rise in free sulfhydryl groups in the protein, facilitating the formation of regular crystals. The three peaks at 43.5°, 44.3°, and 50.5° became flatter, wider, and even disappeared as the RES concentration increased. The addition of RES led to a reduction in the surface hydrophobicity and more hydrophilic groups resulted in a reduction in crystallinity at 40–50°. The protein crystallinity obtained from the simulations is shown in Fig. 4c. The crystallinity of EWP significantly increased ($p < 0.05$) within the RES concentration range of 0 to 0.2 mg/mL. However, upon further increasing the RES concentration, the crystallinity of EWP significantly decreased ($p < 0.05$). In a related study, Ran & Yang[27] explored how varying concentrations of konjac glucomannan affected the crystallinity of soybean isolate protein complexes. The authors observed that the complexes formed ordered crystals, aligning with the findings of the present study.

The TEM results are shown in Fig. 4d. EWP aggregated more significantly and formed larger micelles upon the addition of 50% ethanol (v/v) compared to the control group. Ethanol disrupted the EWP structure, exposing the polar groups, which interacted and caused EWP to aggregate and form nanoparticles. After adding 0.4 mg/mL RES, EWP formed a homogeneous spherical structure, indicating that hydrogen bonds were formed between RES and the exposed polar groups of the EWP, and RES was encapsulated into the interior of the EWP. The reduction in polar group interactions led to decreased aggregation of EWP. This is consistent with the results presented in Fig. 1d and further demonstrates that RES promoted the homogeneity and stability of EWP.

The obtained AFM images are presented in Fig. 4e (dried samples). In the control group, EWP showed irregularity, while the

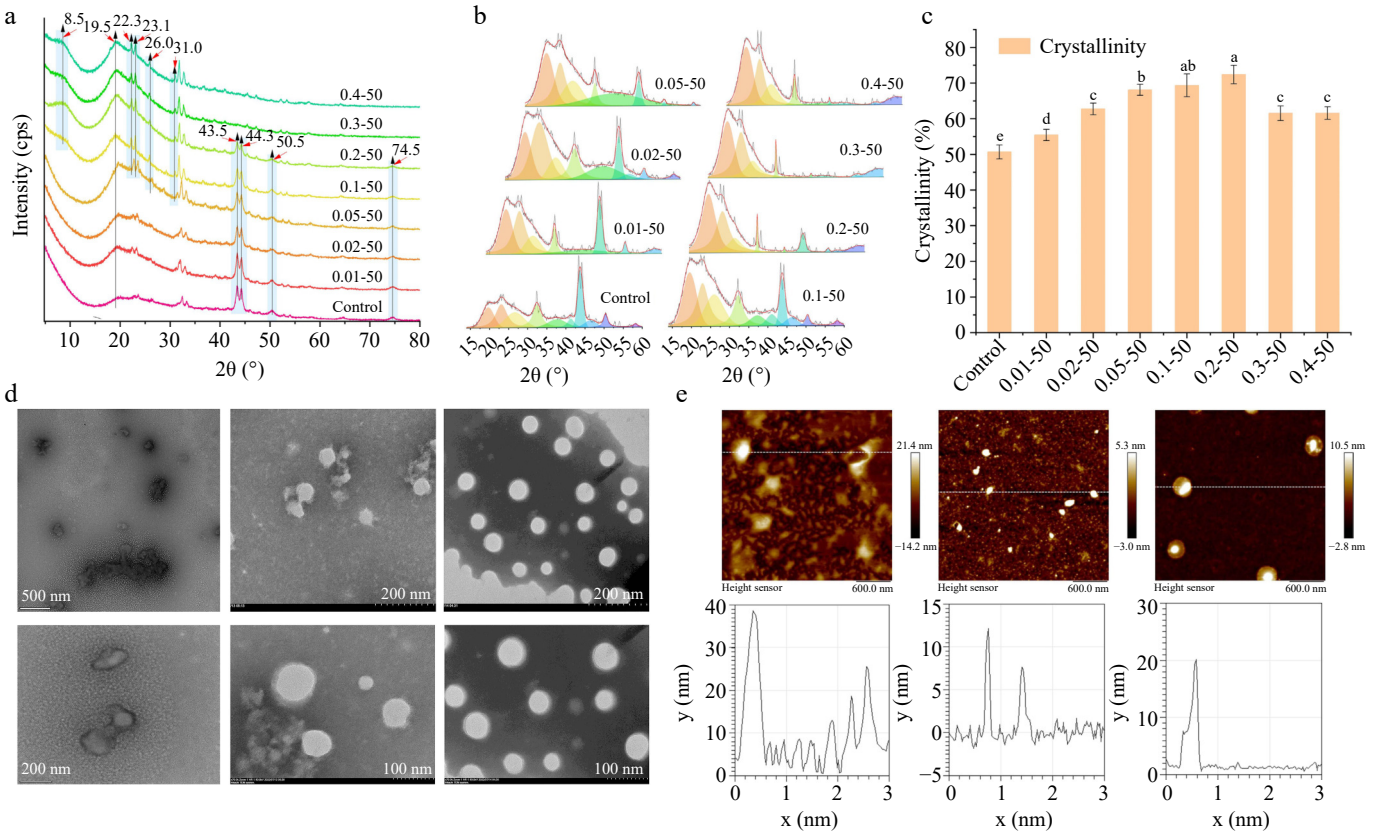

Fig. 4 The (a) XRD spectra, (b) fitted patterns, (c) crystallinity, (d) TEM images, and (e) AFM images and nano height map of ethanol-induced EWP with adding different proportion of RES. The TEM magnifications for control group are 500 and 200 nm, and the for other two groups are 200 and 100 nm. The AFM magnification is 600 nm. Values are given as means ± standard deviation (n = 3). 0.01–50, the preceding digits are RES concentrations (mg/mL), and the following numbers are ethanol concentrations (v/v), other groups are similar. Different letters indicate significant differences between groups ($p < 0.05$).

addition of 50% ethanol significantly reduced the diameter of the EWP particles, dispersing the particles more uniformly and creating a finer structure. Meanwhile, the line scan of the AFM height image showed that the number of height peaks was significantly reduced, and the diameter decreased from 38.7 to 12.5 nm. After adding 0.4 mg/mL of RES, the EWP was more uniformly dispersed, exhibiting spherical nanoparticles and a significant reduction in micelles. The line scan showed only one distinct peak at 20.0 nm, confirming the TEM conclusion that RES prompted EWP to form uniform spherical nanostructures.

Molecular structure analyses of nanoparticles

Raman analysis

Figure 5a displays the Raman spectra of the nanoparticles, covering wavenumbers from 400 to 1,800 cm^{-1}. The 760 cm^{-1} peak signifies the encapsulation of tryptophan residues[28]. A decrease in the absorption peak intensity indicated greater exposure of tryptophan to a polar environment in the nanoparticles. The 1,450 cm^{-1} peak indicates microenvironmental polarity, associated with C-H bending and stretching vibrations of aliphatic amino acid residues[29]. With an increasing concentration of RES, the tryptophan residues predominantly adopted an encapsulated state, and the hydrophobic interactions involving aliphatic amino acid residues were diminished. The amide I (1,600–1,700 cm^{-1}) and amide III (1,230–1,350 cm^{-1}) spectral regions can be analyzed to infer protein secondary structure. At a RES concentration of 0.05 mg/mL, a peak appeared at 1,637 cm^{-1}, indicating increased α-helical content in EWP.

Alterations in the microenvironment of tyrosine residues indicate the exposure of the embedding group, whereas the tyrosine bimodal ratio I_{850}/I_{830} reflects the strength of hydrogen bonding[30]. A ratio between 0.9–2.5 indicates high tyrosine exposure and weak hydrogen bonding[30]. The ratio of I_{850} to I_{830} showed a significant decrease ($p < 0.05$) as the concentration of RES increased (Fig. 5b), indicating that tyrosine residues were encapsulated inside the EWP, while the phenolic group of tyrosine became a hydrogen donor and the strength of the hydrogen bonds increased. Figure 5c illustrates the encapsulation and exposure patterns of tyrosine residues within

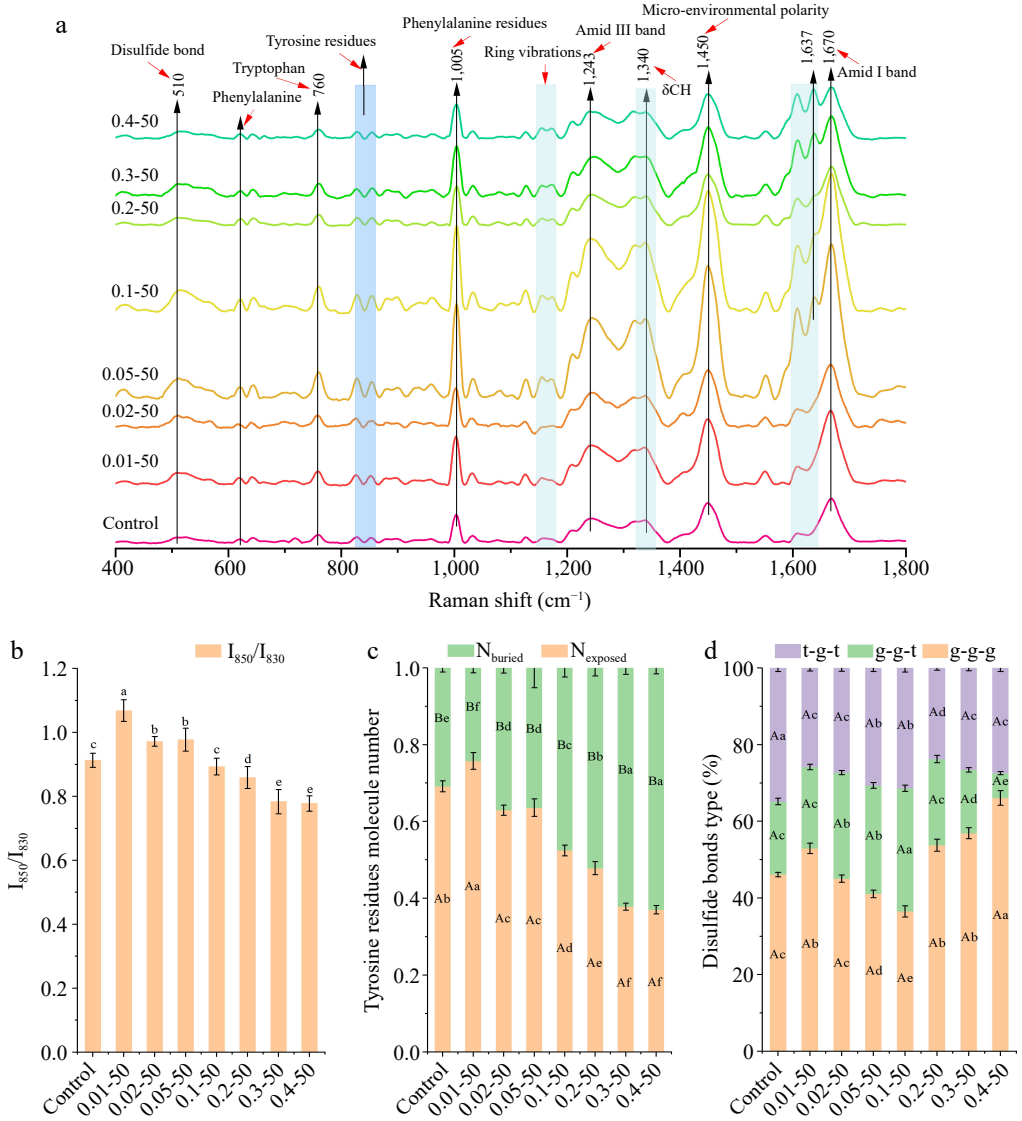

Fig. 5 The (a) Raman shift (400–1,800 cm^{-1}), (b) Tyrosine Fermi resonance line ratio (I_{850}/I_{830}), (c) proportion of exposed and buried tyrosine residues, and (d) different disulfide bond mode ratios of ethanol-induced EWP with adding different proportion of RES. 0.01–50, the preceding digits are RES concentrations (mg/mL), and the following numbers are ethanol concentrations (v/v), other groups are similar. Different letters indicate significant differences between groups ($p < 0.05$).

the nanoparticles. As the concentration of RES increased, there was a tendency for tyrosine residues to become more 'encapsulated', which is in line with the observations presented in Fig. 5b. The introduction of RES resulted in the enhancement of hydrogen bonding strength and the stabilization of helical structures, which in turn led to a reduced exposure of tyrosine residues.

The Raman spectral range of 500–550 cm^{-1} indicates disulfide bonds, with specific conformations identified as gauche-gauche-gauche (500–510 cm^{-1}), gauche-gauche-trans (515–525 cm^{-1}), and trans-gauche-trans (535–545 cm^{-1})[31]. Figure 5d illustrates the impact of ethanol and RES on the disulfide bond conformations in EWP. A notable decrease ($p < 0.05$) in the g-g-g conformation occurred at RES concentrations of 0.01–0.1 mg/mL, while a significant increase ($p < 0.05$) was observed at 0.2 to 0.4 mg/mL. The g-g-t conformation increased to a peak at 0.1 mg/mL of RES before decreasing to a trough at 0.4 mg/mL. The t-g-t conformation significantly decreased ($p < 0.05$) at RES concentrations of 0.01–0.1 and 0.2–0.4 mg/mL, with the control group showing the highest percentage of t-g-t conformations. The incorporation of RES led to the exposure of free sulfhydryl groups, an increase in cross-linking, and alterations in the types of disulfide bonds, which contributed to improved structural elasticity. These findings align with the free sulfhydryl content results shown in Fig. 2a.

FTIR analysis

Figure 6a presents the FTIR spectrum of the nanoparticles. The region between 3,200 and 3,400 cm^{-1} is attributed to the -OH stretching vibrations associated with intermolecular hydrogen bonding[32]. A decrease in the absorption peak at 3,273 cm^{-1} with increasing RES concentration suggests that RES interacts with EWP through hydrogen bonding. The peak at 1,066 cm^{-1} indicates the vibration of C-C and C-O bonds, as well as the bending of the C-H bond[33]. The 518 cm^{-1} peak, indicating C-C skeletal stretching, suggests that RES addition modifies the EWP structure[34]. The amide I band, ranging from 1,700 to 1,600 cm^{-1}, illustrated in Fig. 6b, denotes the protein's secondary structure. With increasing RES concentration, the absorption peaks between 1,600–1,640 cm^{-1} remain unchanged, whereas those in the 1,640–1,650 cm^{-1}, 1,650–1,660 cm^{-1}, and 1,660–1,700 cm^{-1} ranges diminish. This indicates that the interaction between RES and EWP affects its secondary structure.

The secondary structure proportions of EWP were examined using PeakFit 4.12 software, as illustrated in Fig. 6c. The β-sheet, random structure, and β-turn proportions remained stable ($p > 0.05$) at RES concentrations of 0–0.05 mg/mL but significantly decreased ($p < 0.05$) at concentrations of 0.1–0.4 mg/mL. The α-helical content significantly rose ($p < 0.05$) at RES concentrations of 0–0.01 and 0.05–0.1 mg/mL, suggesting a conversion of β-turns to α-helices, which contributed to a stable nanoparticle network structure.

The total hydrogen bonding (THB) within the protein molecule is illustrated in Fig. 6d. THB levels remained unchanged ($p > 0.05$) at RES concentrations of 0–0.05 and 0.1–0.4 mg/mL, except for a significant increase ($p < 0.05$) at 0.1 mg/mL. This suggests that spherical nanoparticles are formed through hydrogen bonding interactions. The protein's three-dimensional structure was determined using the ratio of α-helical to random structures[35]. Figure 6e illustrates the helical/coil ratio of EWP, indicating no significant alterations in the 3D structure at RES concentrations below 0.1 mg/mL ($p > 0.05$). The spatial structure of EWP expanded with a higher RES proportion ($p < 0.05$), suggesting that RES addition promotes cross-linking and the development of a distinct three-dimensional helical structure.

Molecular docking, an effective and straightforward technique, offers comprehensive insights into the interactions between small molecules and biomolecules[36]. Figure 6f illustrates the binding modes and sites of RES and EWP, analyzing the possible interactions. RES formed two hydrogen bonds with Lys19(A) and Ser257(A) residues (binding energies of −3.02 and −3.08 kcal/mol, respectively), and also engaged in hydrophobic interactions with Glu256(A), Glu253(A), Val383(A), Leu252(A), and Asn24(A), Arg381(A). The primary binding forces between RES and EWP are hydrogen bonding and hydrophobic interactions, aligning with FTIR observations of hydrogen bonding (Fig. 6a).

Emulsifying properties of nanoparticles

To assess how varying concentrations of RES influence the interfacial properties of EWP, the surface tension of the nanoparticles was measured, as depicted in Fig. 7a. The surface tension did not significantly change ($p > 0.05$) at RES concentrations below 0.02 mg/mL, but it showed a noticeable decrease ($p < 0.05$) at higher concentrations. This suggests that RES enhances the surface activity of the nanoparticles. Figure 7b illustrates the progressive increase in both the EAI and ESI of EWP with the inclusion of RES ($p < 0.05$). RES decreased the nanoparticles' surface hydrophobicity, promoting hydrogen bond formation between EWP and water molecules. This leads to conformational changes and the extension of the α-helical structure in proteins, thereby increasing the molecular flexibility of the nanoparticles. Consequently, EWP diffused more easily at the oil-water interface, improving emulsification properties. The addition of RES also increased the number of free sulfhydryl groups in the nanoparticles, promoting the diffusion of EWP to the oil-water interface. The covalent interchange between SH and SS groups among interfacial proteins further improved emulsion stability.

Generally, protein-based emulsions are more stable when the average droplet size is smaller, as smaller particles in the emulsion influence the $D_{3,2}$ value[37,38]. Figure 7c illustrates the particle size distributions of emulsions subjected to varying concentrations of RES. Increasing RES concentrations significantly reduced $D_{3,2}$ values ($p < 0.05$), suggesting smaller protein aggregates, reduced droplet size, and enhanced emulsion stability. These findings align with the ESI results presented in Fig. 7b.

The ζ-potential is a crucial and quantifiable indicator for evaluating the stability of emulsions. Emulsions with higher absolute ζ-potential values are considered more stable[38]. It is generally accepted that absolute ζ-potential values exceeding 60 mV indicate exceptional stability of the emulsion system[39]. Figure 7d shows the ζ-potential of the nanoparticles, indicating a significant increase ($p < 0.05$) in the absolute surface charge of EWP from −42.17 to −72.33 mV as the concentration of RES rises. At RES concentrations above 0.05 mg/mL, absolute ζ-potential values exceeded 60 mV, indicating that RES reactive groups increased the negative charge on EWP surfaces, thereby enhancing nanoparticle electrostatic stability. Figure 7e demonstrates a significant increase ($p < 0.05$) in both the interfacial protein content and RES concentration of the nanoparticles. As a phenolic compound, RES can interact with EWP through non-covalent bindings to form protein-polyphenol complexes. Incorporating RES added hydroxyl groups to the nanoparticles, enhancing protein-polyphenol complex adsorption at the oil-water interface. This resulted in an increased content of interfacial protein and interfacial RES, further enhancing the stability of the emulsion system.

Nanoparticle environmental stability

Ionic stability

Figure 8a demonstrates the ionic stability of nanoparticles containing embedded RES. It was evident that the stability of RES incorporated within the nanoparticles significantly declined ($p < 0.05$) with an increase in NaCl concentration across all groups. This suggests that the ionic strength plays a pivotal role in the

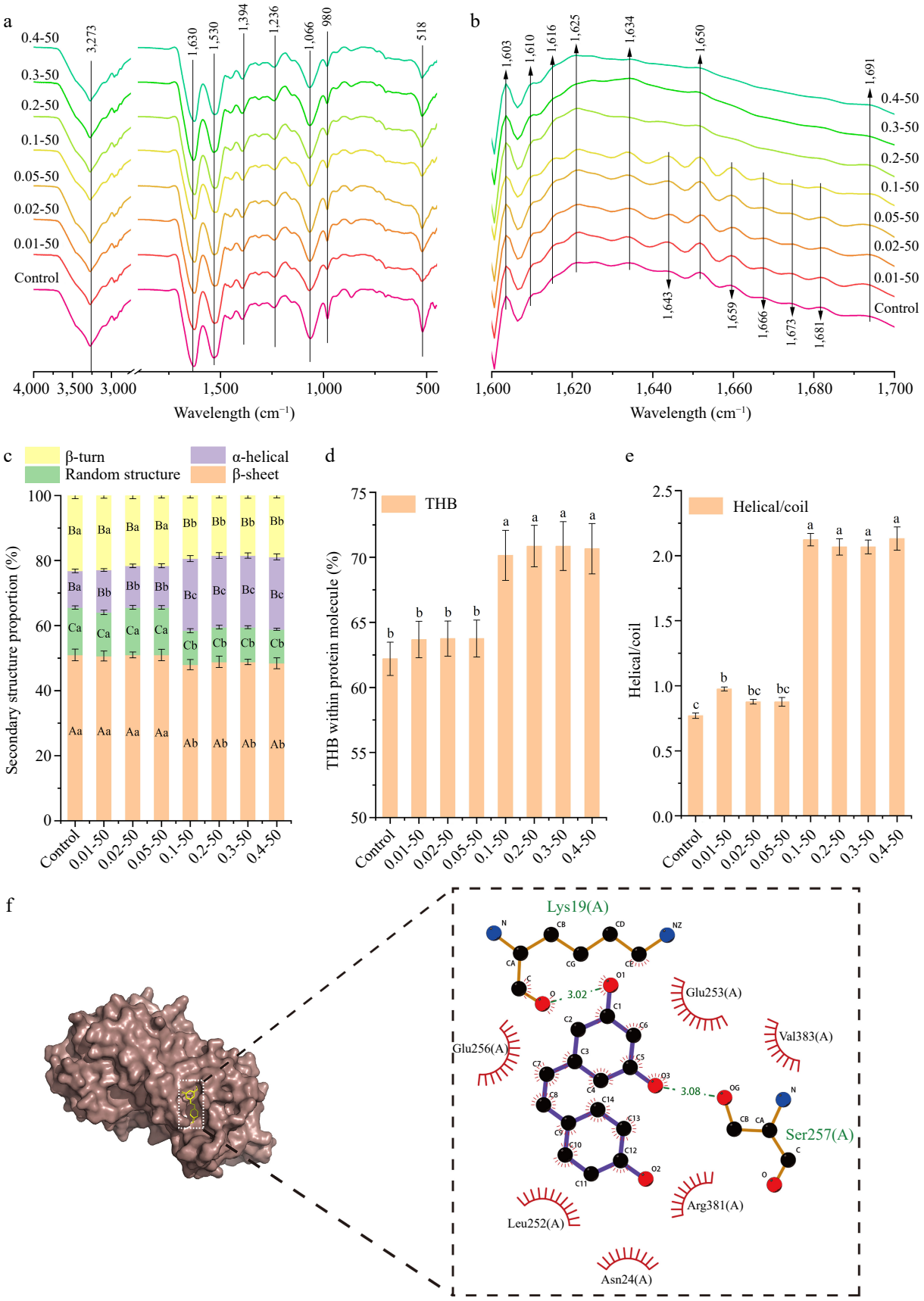

Fig. 6 The (a) FTIR spectra, (b) Fourier self-deconvolved infrared spectra, (c) secondary structure, (d) total hydrogen bonds within protein molecule (THB), (e) helical/coil ratio, and (f) the interaction forces between the amino-acid residues (the green dashed line represents hydrogen bonding forces, red solid line represents hydrophobic force) of ethanol-induced EWP with adding different proportion of RES. 0.01−50, the preceding digits are RES concentrations (mg/mL), and the following numbers are ethanol concentrations (v/v), other groups are similar. Different letters indicate significant differences between groups ($p < 0.05$).

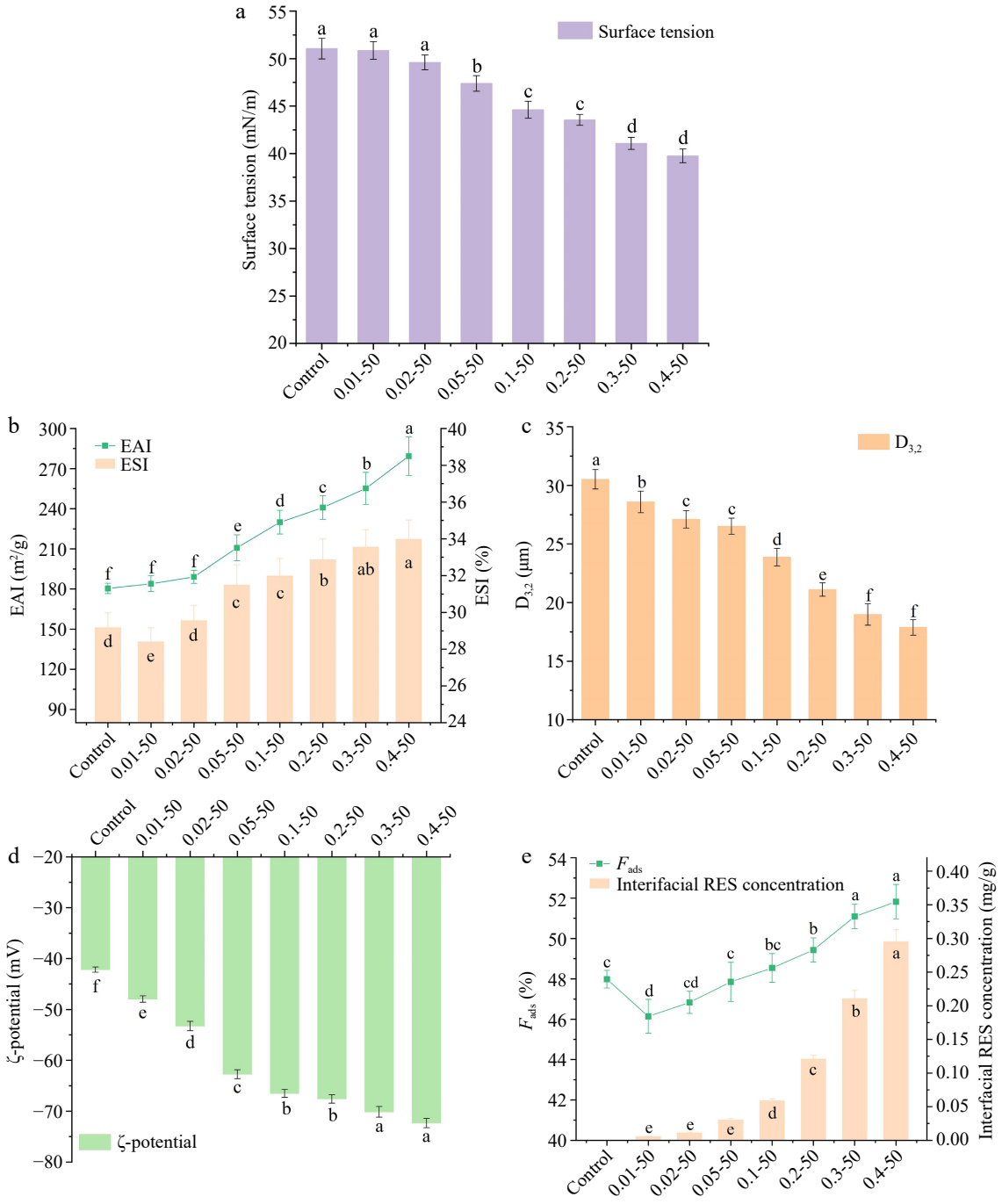

Fig. 7 The (a) surface tension, (b) emulsifying activity index (EAI) and emulsion stability index (ESI), (c) $D_{3,2}$ changes, (d) zeta potential, (e) F_{ads} and interfacial RES concentration of ethanol-induced EWP with adding different proportions of RES. Values are given as means ± standard deviation (n = 3). 0.01-50, the preceding digits are RES concentrations (mg/mL), and the following numbers are ethanol concentrations (v/v), other groups are similar. Different letters indicate significant differences between groups. * means significant difference ($p < 0.05$).

stability of the RES-loaded nanoparticles. For the low RES group, the preservation rate decreased rapidly as compared to the high RES concentration group. For instance, in the 0.01 mg/mL group, RES preservation was 59.53% at 50 mM NaCl and 32.49% at 500 mM NaCl, while for the 0.4 mg/mL group, RES preservation was 94.49% at 50 mM NaCl and 83.68% at 500 mM NaCl. At a constant NaCl concentration, increasing the RES concentration significantly enhanced the RES preservation rate ($p < 0.05$). The addition of NaCl influenced the ambient ion concentration; the electrostatic charge on the protein surface was altered and the protein aggregated. This affected the stability of the active compounds. EWP formed a tighter structure with RES through hydrogen bonding, and RES was encapsulated inside the protein molecule to reduce the outside environment contact. Fu et al.[40] conducted a study where they observed that the Z-average diameter of bovine serum protein-RES nanocomplexes expanded from 33.58 ± 2.97 nm to 95.5 ± 3 nm when NaCl was present, coinciding with a temperature rise from 70 to 90 °C.

Storage stability

Figure 8b shows the activity retention of RES at different storage times. For the lower RES groups (0.01 and 0.02 mg/mL), RES degradation was faster, decreasing from 68.45% at 2 h to 3.31% at 48 h

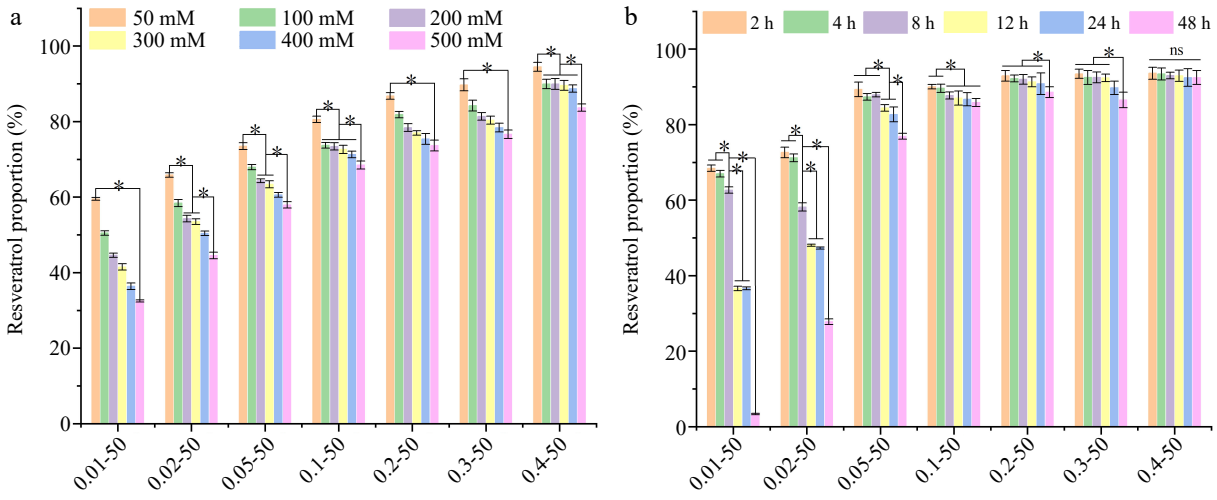

Fig. 8 The (a) ionic stability, and (b) storage stability of ethanol-induced EWP with adding different proportions of RES. 0.01−50, the preceding digits are RES concentrations (mg/mL), and the following numbers are ethanol concentrations (v/v), other groups are similar. Different letters indicate significant differences between groups. * Indicates significant difference ($p < 0.05$).

with the addition of 0.01 mg/mL RES. As the concentration of RES increased, there was a corresponding improvement in its storage stability. Notably, at a concentration of 0.4 mg/mL, the stability of RES remained largely unchanged ($p > 0.05$) throughout a storage period of 48 h. This suggests that EWP formed a better closed spherical network structure with the addition of a high concentration of RES, avoiding the oxidative breakdown of RES due to free exposure to the external environment. Khan et al.[41] encapsulated RES using hollow maize ethanol-soluble protein-chitosan composite particles, enhancing its retention activity at 25 °C from 46% to 78% compared to the control group.

Conclusions

The spherical nanoparticles of EWP with superior dispersion and stability were successfully prepared using a one-step method. Higher concentrations of RES resulted in a better encapsulation rate, ionic environmental stability, and storage stability of the nanoparticle. The addition of RES induced a dynamic quenching of intrinsic fluorescence of EWP through electrostatic interactions, increased the α-helix content, and formed a more stable network structure. The TEM and AFM observations demonstrated that the addition of RES promoted the formation of a uniform spherical structure of EWP. The spherical nanoparticle structure had better structural flexibility, the tyrosine residues tended to be 'encapsulated', the hydrogen bond strength was increased, and the disulfide bond conformation was significantly changed. The addition of RES increased the ζ-potential and decreased the $D_{3,2}$ of the nanoparticles, resulting in better emulsifying activity and emulsion stability. This study establishes a foundation for loading hydrophobic active substances onto EWP. These findings also offer a foundation for a future *in-vivo* activity study of nanoparticles.

Author contributions

The authors confirm contribution to the paper as follows: study conception and design, draft manuscript preparation: Kang Y; formal analysis: Kang Y, Xiao N; investigation: Xiao N, Wu H, Pan Z, Chen W; manuscript revision and editing, resources, project supervision: Ai M. All authors reviewed the results and approved the final version of the manuscript

Data availability

All data generated or analyzed during this study are included in this published article and its supplementary information files.

Acknowledgments

The authors are thankful for the financial support from Guangzhou 2023 basic and applied basic research topics (2023A04J1468); The National Center for Precision Machining and Safety of Livestock and Poultry Products Joint Engineering Research Center (2016(2203)), China, and the Guangdong Provincial Key Laboratory of Food Quality and Safety (2020B1212060059).

Conflict of interest

The authors declare that they have no conflict of interest.

Supplementary information accompanies this paper at (https://www.maxapress.com/article/doi/10.48130/fia-0025-0001)

Dates

Received 2 August 2024; Revised 16 October 2024; Accepted 4 December 2024; Published online 20 January 2025

References

1. Davidov-Pardo G, McClements DJ. 2014. Resveratrol encapsulation: Designing delivery systems to overcome solubility, stability and bioavailability issues. *Trends in Food Science & Technology* 38:88−103
2. Zupančič Š, Lavri č Z, Kristl J . 2015. Stability and solubility of trans-resveratrol are strongly influenced by pH and temperature. *European Journal of Pharmaceutics and Biopharmaceutics* 93:196−204
3. Liazid A, Palma M, Brigui J, Barroso CG. 2007. Investigation on phenolic compounds stability during microwave-assisted extraction. *Journal of Chromatography A* 1140:29−34
4. Chen S, Zhang Y, Han Y, McClements DJ, Liao W, et al. 2020. Fabrication of multilayer structural microparticles for co-encapsulating coenzyme Q10 and piperine: Effect of the encapsulation location and interface thickness. *Food Hydrocolloids* 109:106090
5. Peñalva R, Morales J, González-Navarro CJ, Larrañeta E, Quincoces G, et al. 2018. Increased oral bioavailability of resveratrol by its encapsulation in casein nanoparticles. *International Journal of Molecular Sciences* 19:2816

6. Jalili-Firoozinezhad S, Filippi M, Mohabatpour F, Letourneur D, Scherberich A. 2020. Chicken egg white: Hatching of a new old biomaterial. *Materials Today* 40:193–214
7. Sun Y, Jin H, Sun H, Sheng L. 2020. A comprehensive identification of chicken egg white phosphoproteomics based on a novel digestion approach. *Journal of Agricultural and Food Chemistry* 68:9213–22
8. Kleemann C, Schuster R, Rosenecker E, Selmer I, Smirnova I, et al. 2020. In-vitro-digestion and swelling kinetics of whey protein, egg white protein and sodium caseinate aerogels. *Food Hydrocolloids* 101:105534
9. Zhu H, Mettu S, Cavalieri F, Ashokkumar M. 2021. Ultrasonic microencapsulation of oil-soluble vitamins by hen egg white and green tea for fortification of food. *Food Chemistry* 353:129432
10. Zhang Y, Guo Y, Liu F, Luo Y. 2023. Recent development of egg protein fractions and individual proteins as encapsulant materials for delivery of bioactives. *Food Chemistry* 403:134353
11. Yao L, Jiang A, Chen L. 2020. Characterization of ethanol-induced egg white gel and transportation of active nutraceuticals. *LWT* 130:109530
12. Avramenko NA, Low NH, Nickerson MT. 2013. The effects of limited enzymatic hydrolysis on the physicochemical and emulsifying properties of a lentil protein isolate. *Food Research International* 51:162–69
13. Trott O, Olson AJ. 2010. AutoDock Vina: Improving the speed and accuracy of docking with a new scoring function, efficient optimization, and multithreading. *Journal of Computational Chemistry* 31:455–61
14. Ni Y, Wen L, Wang L, Dang Y, Zhou P, et al. 2015. Effect of temperature, calcium and protein concentration on aggregation of whey protein isolate: formation of gel-like micro-particles. *International Dairy Journal* 51:8–15
15. Aguiar J, Carpena P, Molina-Bolívar JA, Carnero Ruiz C. 2003. On the determination of the critical micelle concentration by the pyrene 1:3 ratio method. *Journal of Colloid and Interface Science* 258:116–22
16. Filip V, Plocková M, Šmidrkal J, Špičková Z, Melzoch K, Schmidt Š. 2003. Resveratrol and its antioxidant and antimicrobial effectiveness. *Food Chemistry* 83:585–93
17. Liu LL, Li XT, Zhang N, Tang CH. 2019. Novel soy β-conglycinin nanoparticles by ethanol-assisted disassembly and reassembly: outstanding nanocarriers for hydrophobic nutraceuticals. *Food Hydrocolloids* 91:246–55
18. Wang JY, Yang YL, Tang XZ, Ni WX, Zhou L. 2017. Effects of pulsed ultrasound on rheological and structural properties of chicken myofibrillar protein. *Ultrasonics Sonochemistry* 38:225–33
19. Wang Z, Xiao N, Guo S, Tian X, Ai M. 2024. Tea polyphenol-mediated network proteins modulate the NaOH-heat induced egg white protein gelling properties. *Food Hydrocolloids* 149:109514
20. Mune Mune MA, Sogi DS. 2015. Functional Properties of Protein Concentrates of Cowpea and Bambara Bean Involving Different Drying Techniques. *Journal of Food Processing and Preservation* 39:2304–13
21. Wang C, Li J, Li X, Chang C, Zhang M, et al. 2019. Emulsifying properties of glycation or glycation-heat modified egg white protein. *Food Research International* 119:227–35
22. Cheng H, Fang Z, Bakry AM, Chen Y, Liang L. 2018. Complexation of *trans*-and *cis*-resveratrol with bovine serum albumin, β-lactoglobulin or α-lactalbumin. *Food Hydrocolloids* 81:242–52
23. Bustos LF, Judis MA, Vasile FE, Pérez OE. 2022. Molecular interactions involved in the complexation process between buffalo whey proteins concentrate and folic acid. *Food Chemistry* 396:133734
24. Chen H, Jin Y, Ding X, Wu F, Bashari M, et al. 2014. Improved the emulsion stability of phosvitin from hen egg yolk against different pH by the covalent attachment with dextran. *Food Hydrocolloids* 39:104–12
25. Zhong Y, Yang L, Dai T, Zhu Z, Chen H, et al. 2022. Flavonoids enhance gel strength of ovalbumin: Properties, structures, and interactions. *Food Chemistry* 387:132892
26. Liu Y, Ying D, Cai Y, Le X. 2017. Improved antioxidant activity and physicochemical properties of curcumin by adding ovalbumin and its structural characterization. *Food Hydrocolloids* 72:304–11
27. Ran X, Yang H. 2022. Promoted strain-hardening and crystallinity of a soy protein-konjac glucomannan complex gel by konjac glucomannan. *Food Hydrocolloids* 133:107959
28. Xu XL, Han MY, Fei Y, Zhou GH. 2011. Raman spectroscopic study of heat-induced gelation of pork myofibrillar proteins and its relationship with textural characteristic. *Meat Science* 87:159–64
29. Bouraoui M, Nakai S, Li-Chan E. 1997. In situ investigation of protein structure in Pacific whiting surimi and gels using Raman spectroscopy. *Food Research International* 30:65–72
30. Howell N, Li-Chan E. 1996. Elucidation of interactions of lysozyme with whey proteins by Raman spectroscopy. *International Journal of Food Science & Technology* 31:439–51
31. Herrero AM. 2008. Raman spectroscopy for monitoring protein structure in muscle food systems. *Critical Reviews in Food Science and Nutrition* 48:512–23
32. Jiménez A, Sánchez-González L, Desobry S, Chiralt A, Tehrany EA. 2014. Influence of nanoliposomes incorporation on properties of film forming dispersions and films based on corn starch and sodium caseinate. *Food Hydrocolloids* 35:159–69
33. Jackson M, Mantsch HH. 1995. The use and misuse of FTIR spectroscopy in the determination of protein structure. *Critical Reviews in Biochemistry and Molecular Biology* 30:95–120
34. Ai M, Jiang A. 2021. Phosphorylation modification affects the gelation behavior of alkali-induced duck egg white gels. *Food Chemistry* 340:128185
35. Sow LC, Peh YR, Pekerti BN, Fu C, Bansal N, et al. 2017. Nanostructural analysis and textural modification of tilapia fish gelatin affected by gellan and calcium chloride addition. *LWT* 85:137–45
36. Mahmoudpour M, Javaheri-Ghezeldizaj F, Yekta R, Torbati M, Mohammadzadeh-Aghdash H, et al. 2020. Thermodynamic analysis of albumin interaction with monosodium glutamate food additive: Insights from multi-spectroscopic and molecular docking approaches. *Journal of Molecular Structure* 1221:128785
37. McClements DJ. 2007. Critical Review of Techniques and Methodologies for Characterization of Emulsion Stability. *Critical Reviews in Food Science and Nutrition* 47:611–49
38. Şen L, Okur S. 2023. Effect of hazelnut type, hydrocolloid concentrations and ultrasound applications on physicochemical and sensory characteristics of hazelnut-based milks. *Food Chemistry* 402:134288
39. Mahbubul IM, Chong TH, Khaleduzzaman SS, Shahrul IM, Saidur R, et al. 2014. Effect of ultrasonication duration on colloidal structure and viscosity of alumina–water nanofluid. *Industrial & Engineering Chemistry Research* 53:6677–84
40. Fu JJ, Zhang GY, Zhang ZH, Shao ZW, Xu XB, et al. 2022. Formation mechanism of nanocomplex of resveratrol and glycated bovine serum albumin and their glycation-enhanced stability showing glycation extent. *LWT* 155:112916
41. Khan MA, Chen L, Liang L. 2021. Improvement in storage stability and resveratrol retention by fabrication of hollow zein-chitosan composite particles. *Food Hydrocolloids* 113:106477